 doi:10.20944/preprints201805.0442.v1

Article

COSMO–SkyMed Synthetic Aperture Radar data to observe the Deepwater Horizon oil spill

Ferdinando Nunziata [1,*], Andrea Buono [1,*] and Maurizio Migliaccio [1,*]

[1] Università degli Studi di Napoli Parthenope, Dipartimento di Ingegneria; nunziata,andrea.buono,migliaccio@uniparthenope.it

* Correspondence: {nunziata,andrea.buono,migliaccio}@uniparthenope.it; Tel.: +39-081-547-6768

Abstract: Oil spills are adverse events that may be very harmful to ecosystems and food chain. In particular, large sea oil spills are very dramatic occurrence often affecting sea and coastal areas. Therefore the sustainability of oil rig infrastructures and oil transportation via oil tankers are linked to law enforcement based on proper monitoring techniques which are also fundamental to mitigate the impact of such pollution. Within this context, in this study a meaningful showcase is analyzed using remotely sensed measurements collected by by Synthetic Aperture Radar (SAR) satellites. The Deepwater Horizon (DWH) oil accident that occurred in the Gulf of Mexico in 2010 is here analyzed. It is one of the world's largest accidental oil pollution event that affected a sea area larger than 10,000 km^2. In this study we exploit SAR data collected by the Italian COSMO–SkyMed (CSK) X–band SAR constellation showing the key benefits of multi–polarization HH–VV SAR measurements in observing such a huge oil pollution event.

Keywords: Sea, remote sensing, oil pollution

1. Introduction

Oceans, seas and all the marine resources are essential to human well–being and social and economic development [1]. Oceans provide livelihoods, subsistence and benefits from fisheries, tourism and many other sectors, also helping in regulating the global ecosystem by absorbing heat and carbon dioxide from the atmosphere. However, oceans and coastal areas are severely susceptible to environmental degradation, overfishing, climate change, biodiversity loss and pollution [2]. In particular, pollutants significantly threat coastal regions and, since river basins, marine ecosystems and the atmosphere belong all together to the same hydrological systems, its effects are often found at far distance by the polluting source. According to the 2015 "Transboundary Waters Assessment Programme" global comparative assessment, the Gulf of Mexico is one of the five largest marine ecosystems mostly at risk of pollution and eutrophication. Hence, its preservation and sustainable management are key points to be achieved in the 2030 Agenda [3]. One of the goals mentioned in the sustainable development report of 2016 explicitly states "conserve and sustainably use the oceans, seas and marine resources for sustainable development" is of primary importance [4].

Sea oil spills are the most noticeable forms of damage to the marine environment. Oil at sea comes from oil tanker or oil rig disasters, but also — and primarily — from diffuse sources, such as leaks during oil extraction, illegal tank–cleaning operations at sea, or discharges into the rivers which are then carried into the sea. Generally speaking, two classes of sea oil spill may occur, large oil spills and small oil spills. In the first case, we are dealing with macro oil spills; while in the second case we have micro oil spills. The size and duration of the spill, its chemical makeup and the marine environment are key factors to evaluate the short– and long–term ecological consequences of the spillage. While macro oil spills are well–known in general terms, the correct monitoring of the time evolving processes

 doi:10.20944/preprints201805.0442.v1

and the precise knowledge of the marine and coastal area affected is crucial. Micro oil spills are usually much more difficult to be monitored by patrol coast guard ships and airplanes, since they represent small–size events that may occurr in a large areas.

Although proper monitoring is only the first part of a challenging scientific and operational processing chain it is important to be properly made [5]. In fact, although any macro oil spill has its unique characteristics, the logic processing chain is based on some key functional tools: monitoring, forecasting and vulnerability assessment. It must be noted that many uncertainties still remain especially in forecasting of an oil spill because of meteo–marine conditions and aging that make oil forecasting a complex process that cannot be standardized in a simple way. Hence, it is important to provide to the forecast modeler the best available information in terms of sea oil coverage and possibly sea oil type. Sea oil type has a direct impact on forecasting since when oil has a predominant component that is volatile the polluting contamination process is very different with respect to the case where heavy damping oil is predominant. Generally speaking, in order to mitigate the adverse effects of a sea oil spill, it is a paramount importance to monitor the event and to provide the best information to the operational people to support remediation actions and dispatch proper bulletin to fishermen and population [6].

With reference to oil tanker security, especially after the Prestige accident in 2002, the use of double–hull tankers was meant as the primary source to limit the risk of accidents. Unfortunately, the recent Sanchi accident in 2018 demonstrated that this ship construction technology does not lead to zero risk. On the other side, oil rigs are more and more environmental risky as they move to deep and ultra–deep sea. The reference accident is the Deepwater Horizon (DWH) accident that occurred in 2010 in the Gulf of Mexico [7,8]. The oil spill industry sustainability is based on the increasing and increasing sea oil spill remediation capability and this is also based on the quality of the monitoring capability.

In this framework, this study focuses on the benefit of satellite day–and–night high–resolution Synthetic Aperture Radar (SAR) monitoring during the DWH accident. In fact, among the various remote sensing tools, SAR could effectively address the user needs in case of such huge accidental polluting events in terms of:

- area covered;
- continuous and almost near real–time operability.

SAR imaging characteristics provide several extra–benefits if compared to optical remote sensing, even though the latter is extensively used to retrieve rough estimations of oil thickness and chemical properties. However, optical measurements are severely affected by weather conditions and, furthermore, response efforts as the use of chemical dispersants, may alter oil slicks' appearance by dispersing it in subsurfaces making the interpretation of optical data non–trivial at all [5,6].

It is internationally recognized that oil spill response operational services obtain great benefits by utilizing airborne/satellite-based remote sensing for oil spill surveillance [9,10]. In fact, several countries and governmental agencies, e.g. the European Maritime Safety Agency, assist their operational services by providing remotely sensed measurements, especially by SAR imagery. The latter is an active, coherent, band–limited microwave high–resolution sensor that can make day– and night–time measurements almost independently of atmospheric conditions. Among the currently available SAR systems, the Italian COSMO–SkyMed (CSK) one is attractive from an operational point of view since it is a constellation of four X–band SARs, characterized by a very short revisit time, i. e., $\approx$ 12 hours, and it is able to operate in an incoherent dual–polarization mode (Ping Pong, PP, mode). The capability of CSK to support an operational monitoring of the oceans have been demonstrated in [11,12,13].

SAR oil slick observation is physically possible because an oil slick damps the short gravity and capillary waves which are responsible for the backscattering to the SAR antenna and therefore a low backscattering return occurs. As a result, in the SAR image plane, a dark area is associated to an oil slick [14]. SAR oil spill detection is not an easy task, since SAR images are affected by multiplicative noise,

 doi:10.20944/preprints201805.0442.v1

known as speckle, which hampers the interpretability of such images. Furthermore, there are other physical phenomena, known as look–alikes, which can generate dark areas in SAR images not related to oil spills, such as biogenic films, low–wind areas, rain cells, internal waves and oceanic or atmospheric fronts [15]. Accordingly, tailored filtering techniques must be developed in order to minimize the number of false alarms. They are generally based on the use of single–polarization SAR data together with ancillary data [5,14,16]. In some cases, the distinction between oil slicks and biogenic films is based on optical data [5]. The importance of dual–polarization SAR measurements has been demonstrated in literature for oil slicks observation purposes [17,18,19]. Nevertheless, although it has been physically demonstrated by theoretical modelling and experiments that polarimetric SAR measurements are the most adequate source to monitor oil slicks at sea [10,20], it is important to analyze, especially in the occurrence of large oil spill accidents, how all the available SAR measurements can be exploited at best.

In this study a multi–polarization analysis of the capabilities of dual–polarization PP mode X–band CSK SAR data is first undertaken focusing on the DWH oil spill. The latter was extensively monitored by means of L–, C– and X–band SAR systems but, to the best of our knowledge, no study exploited the incoherent CSK PP mode to consider such a huge oil spill event [21,22,23,24]. Oil spill detection and estimation of the polluted area is undertaken using a textural–based image processing approach, while a multi–polarization analysis is undertaken in order to characterize the contrast, i. e., the ratio between the Normalized Radar Cross Section (NRCS) relevant to the slick–free and oil–covered sea surface, both in the HH and VV channels.

Experiments, accomplished over X–band HH–VV PP mode Single–look Complex Slant (SCS) Level 1A CSK SAR data collected in the Gulf of Mexico over the polluted area, demonstrate the importance of the Italian constellation of CSK SAR satellites for an effective observation of sea oil slicks.

2. The Deepwater Horizon accidental oil spill: a case study

On 20 April 2010, a fire broke out on the Transocean DWH oil rig under lease to British Petroleum (BP), with 126 people on board (see Figure 1 (a)). After a large explosion, all but 11 of the crew managed to escape as the rig was overwhelmed by fire. On 22 April 2010, the rig sank. Safeguards set in place to automatically cap the oil well in case of catastrophe did not work as expected. According to a first conservative Minerals Management Service formula, BP estimated at worst a spill of 162,000 barrels per day and a standard technology recovery capacity of about 500,000 barrels per day. Only after 12 weeks did BP succeed in placing a tight cap on the well. A first estimate of about 5 million barrels [25,26] already makes this accident the world's largest accidental oil spill and, by far, the worst oil disaster in United States history. It is surpassed only by the intentional 1991 Gulf War spill in Kuwait. Oil spilled from the DWH wellhead was a Mississippi Canyon Block 252 (MS252) South Louisiana sweet, i. e., low in sulfur concentration, crude oil and, as far as for all the crude oils, it consists of thousands of chemical compounds [25,26]. The vast and persistent DWH spill challenged response capabilities which called for quantitative oil assessment at synoptic and operational scales. Although nowadays oil spill response still mainly relies on experienced observers, few trained observers and confounding factors, including weather, oil emulsification and scene illumination geometry presented very non-trivial challenges [7,27]. Moreover, the DWH spill was characterised by some key peculiarities that made its observation very challenging:

- the spill originated from a water–depth of 1500 m. This has confounded many problems on understanding the behaviour of the oil [28,29]. In general, oil at sea is influenced by a number of advective processes, e.g. wind and wave advection, spreading, etc., and weathering. The latter is a non–advective process that alters the oil's chemical and physical properties. In addition to the conventional weathering process on the surface, the DWH oil was subjected to weathering as it ascended from the well. In fact, DWH oil appeared to be incorporating water as it emerged on the surface [28,29];

Preprints (www.preprints.org) | NOT PEER-REVIEWED | Posted: 30 May 2018 doi:10.20944/preprints201805.0442.v1

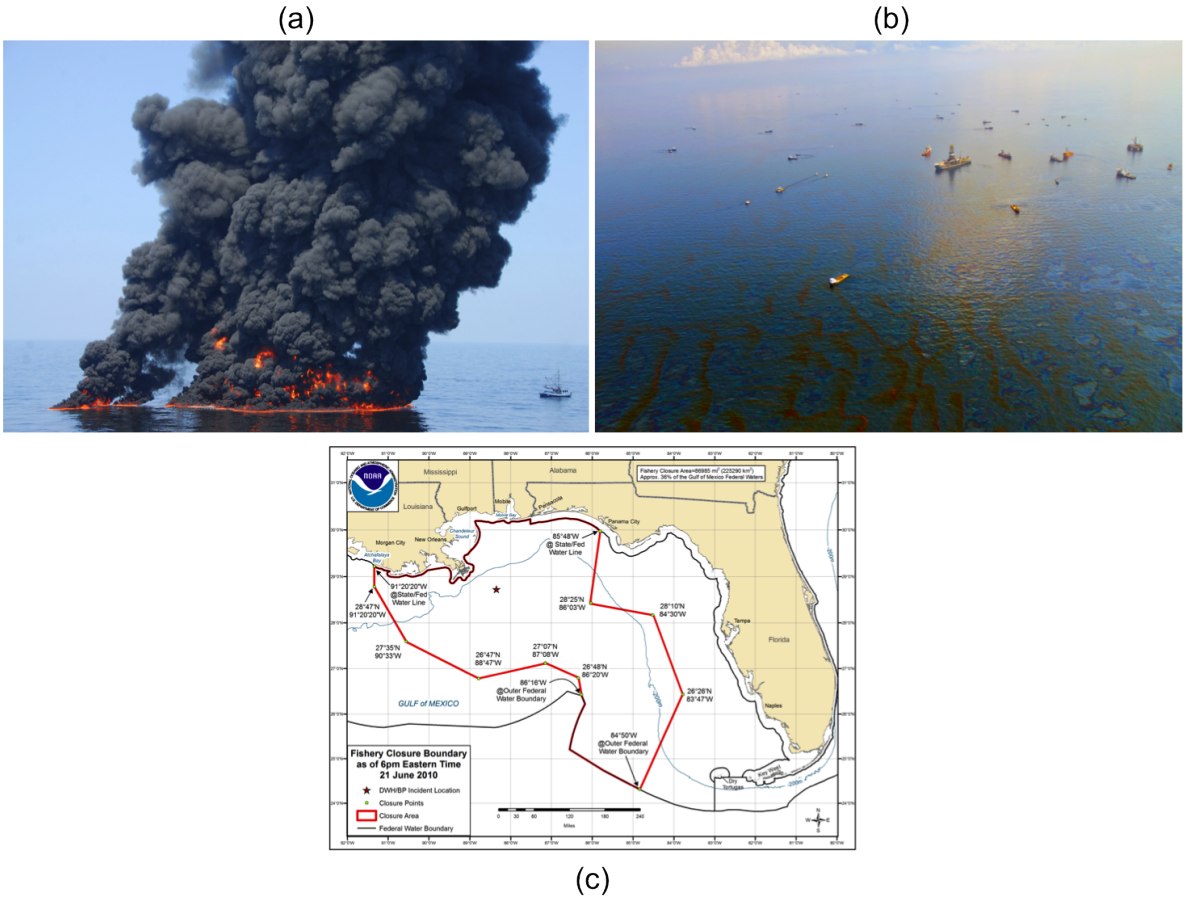

Figure 1. The DWH oil spill accident. (a) Burning of the BP DWH oil rig; (b) Remediation activities; (c) Fishery clousure boundaries 1 day after the accident (courtesy of NOAA).

- fresh oil was continuously released. Unlike "conventional" tankers oil spills, where oil is released at once, the DWH oil spill was far more challenging due to continuous fresh oil release. Hence, in a continuous release situation there is a mixture of fresh and weathered oil (of various degrees) as well as emulsified oil;

- a massive use of dispersants was made to mitigate the oil's impact on the environment [26,28]. The dispersants help to reduce the oil–water interfacial tension which, when aided by the addition of energy in the form of wind/waves, can help to enhance natural dispersion of the oil. During the DWH oil spill, nearly 2 million of gallons of chemical dispersant were used both on the surface and directly onto the gushing oil at the wellhead in an attempt to keep some of the oil under the water surface (see Figure 1 (b)). Scientists believe that BP's excessive use of dispersants have contributed significantly to the enormous underwater oil plumes that remain in the Gulf, one of which was 22 miles long and six miles wide [26,28];

- the polluted area was very large (10,000km^2), see Figure 1 (c) [25]. This hampered traditional approaches to provide a synoptic spill observation, thus making remote sensing a key asset [30].

In addition, such huge oil spillage may have a critical long–term impact over the whole marine and coastal ecosystem and, therefore, still needs to be continuosly monitored [31,32].
In summary, this unprecedented oil spill accident triggered the operational use of SAR techniques to provide detailed information on the surfactants related to the DWH accident. Nevertheless, since the DWH polluted area includes oil slicks of different thickness, emulsified oil, weathered

 doi:10.20944/preprints201805.0442.v1

oil, oil/dispersant mixture, fresh oil, etc., the surface slick is very heterogeneous, including different kind of surfactants. This implies that a synergistic use of different SAR operating modes is needed. In fact, large–swath imaging modes, i. e., ScanSAR, allow obtaining information on the extent of the oil spill, while narrower swath polarimetric modes, i. e., PP, allow extracting deeper information on the oil's backscattering.

3. Experiments and discussion

In this section experiments undertaken on multi–polarization SCS CSK SAR data collected over the Gulf of Mexico area affected by the DWH accident are presented and discussed to demonstrate their potential in detecting the oil spill and to analyze the slick–free and oil–covered sea surface backscattering under different polarizations.

The CSK SAR data set consists of two SAR scenes collected in right–looking ascending orbit over the DWH accidental oil spill site in the very next days after the accident, see Figure 2. The first SAR scene (product ID: 2006020) was acquired from the satellite "3" of the constellation on April 23, 2010, i. e., only 3 days after the oil spillage just after the BP oil rig sank, in dual–polarization HH–VV PingPong mode under an incidence angle of 40° at mid–range. The SAR image consists of a 4123 $\times$ 18042 pixels covering an area of 30 km $\times$ 30 km with about 5 m $\times$ 2 m (range $\times$ azimuth) spatial resolution.

A key parameter when observing sea oil slicks by SAR imagery is wind speed. In fact, it is unanimously recognized that SAR oil slick observation is possible when moderate wind conditions, i. e., wind speed ranges from about 2 m/s up to approximately 13 m/s [9,33]. When higher wind conditions apply, mixing phenomena dominate making the detectability of oil with respect to the surrounding sea impossible. At lower wind speeds, sea surface backscattering is comparable to the scattering from the oil slick; hence, even in this case oil–sea separability is not possible. Typically wind information is provided by ancillary remotely sensed data, e. g., scatterometer/radiometer or buoy measurements. Unfortunately, very often the information coming from other remotely sensed sources is not co–located in time and/or space with the available SAR data set. In addition, buoys co–located to the accident point are not always available.

Hence, in this study a different approach is proposed that consists of providing a wind map by processing the SAR image. Different methods are available in literature that are mainly based on the exploitation of a scatterometer–like Geophsyical Model Function (GMF) to extract wind speed information once a priori wind direction information is available [34,35,36]. In this study, a spectral approach is considered that does not require any a priori wind direction information to provide the wind speed map. This approach is based on the inherent SAR peculiarities, i. e., the low–pass filtering in the azimuth direction due to the orbital motion of the sea surface waves that distorts the Doppler history of the backscattered waves [37,38]. The wind map, generated using the azimuth cut–off method, is shown in Figure 3 where the oil–covered area is masked out. It can be noted that low–to–moderate wind regime applies that is characterized by a mean wind speed of 7 m/s at the SAR acquisition time. Hence, SAR sea oil slick detection can be effectively undertaken.

3.1. Oil spill detection

In this subsection a texture–based oil spill detection procedure is undertaken to assess the potential of CSK SAR data to detect the DWH oil spill and to estimate its surface extent.

In order to extract suitable intensity–based features that allow obtaining the oil spill detection binary mask, a textural–based feature extraction algorithm is adopted using the Gray–Level Co–occurrence Matrix (GLCM). The latter is one of the most popular statistical method to extract second–order texture features from remotely sensed images. The technique has been already successfully exploited in a broad range of SAR applications, e. g., ice–cover classification [39] and oil detection [40]. Basically, GLCM is a mathematical formalism that takes into account how often different pixel intensity value combinations occur in a remotely sensed image within given distances and directions. Among the basic GLCM parameters that can be extracted from a SAR image, which include mean, variance, correlation,

Preprints (www.preprints.org) | NOT PEER-REVIEWED | Posted: 30 May 2018 doi:10.20944/preprints201805.0442.v1

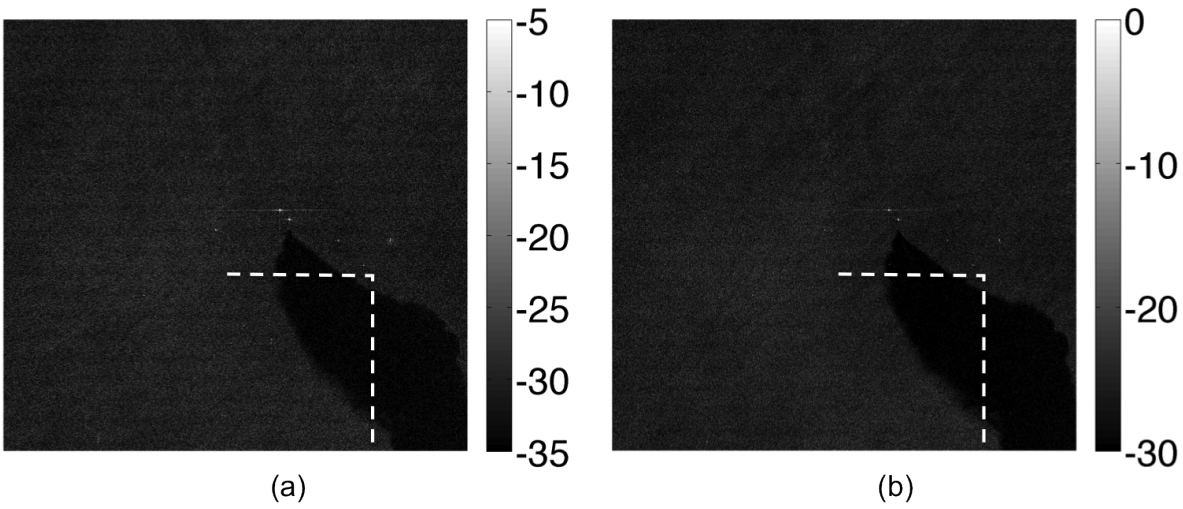

Figure 2. Multi–polarization CSK SAR imagery relevant to the acquisition collected on 23 April 2010. (a) HH– and (b) VV–polarized NRCS graytone images (dB scale).

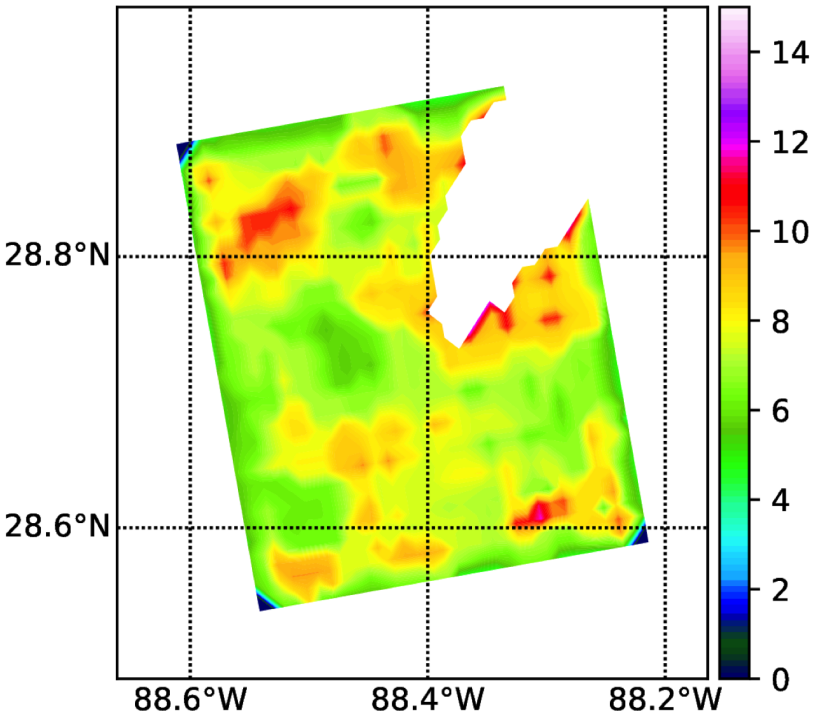

Figure 3. Azimuth cut–off based wind speed map derived from the CSK SAR scene collected on 23 April 2010.

Preprints (www.preprints.org) | NOT PEER-REVIEWED | Posted: 30 May 2018 doi:10.20944/preprints201805.0442.v1

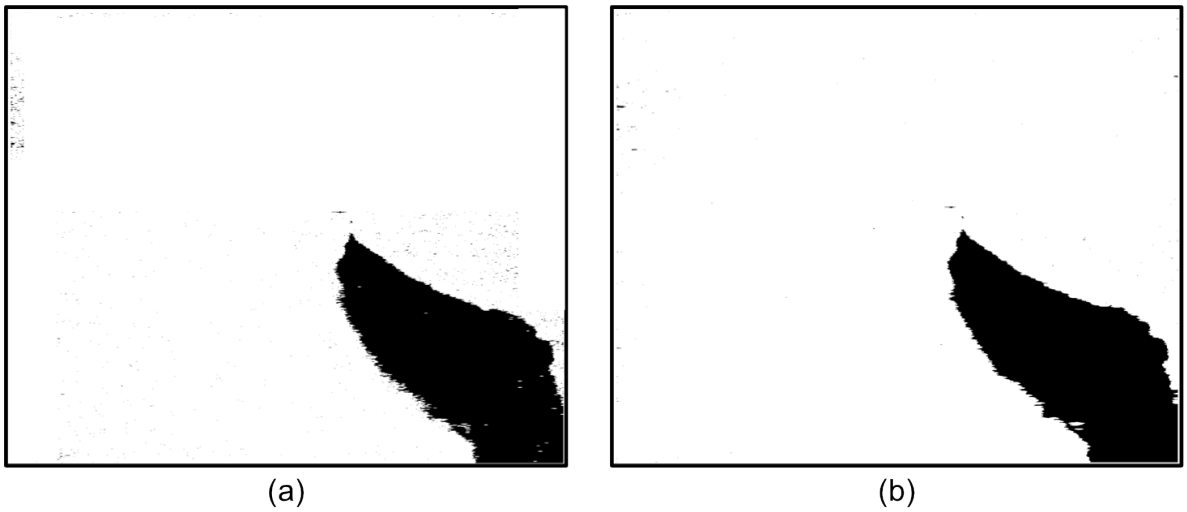

Figure 4. ASM–based oil detection maps relevant to the CSK SAR scene collected on 23 April 2010. (a) HH and (b) VV channel.

entropy, homogeneity, energy, contrast, dissimilarity, etc., the Angular Second Moment (ASM) was found to be the most effective in separating the oiled area from the surrounding sea. ASM is defined as $\sum_{i,j=0}^{N}[I(i,j)]^2$, where P is the original intensity SAR image and N is the number of gray levels [41]. ASM can be seen as a measure of homogeneity of the intensity SAR image. Since the oiled area is expected to be more homogeneous than the sea surface, i. e., few gray levels are present, it will be characterized by few and relatively high intensity values $I(i,j)$ that result in ASM values larger than the ones characterizing sea surface. In this study, quantization in $N = 32$ gray levels and a 9×9 sliding window are used to estimate ASM.

Oil spill detection results are shown in Figure 4, where the binary masks obtained thresholding the ASM images are obtained from HH and VV channel (see Figure 4 (a) and (b), respectively). A threshold ASM = 1 is empirically set. Post–processing techniques, i. e., a morphological filter, is then applied to derive the oil detection maps of Figure 4. It can be noted that the oil detection mask obtained from the VV NRCS clearly separates the polluted area, that calls for ASM values larger than 1 due to its homogeneity, from the surrounding sea, that represents a more heterogeneous scenarios resulting in a lower ASM values (see Figure 4 (b)). Please note also that the few isolated black spots related to metallic targets at sea involved in cleaning–up operations (see bright spots in Figure 2) are visible in the oil spill detection map. This is likely due to the fact that they behave as very homogeneous scatterers. The oil spill can be detected even from the HH NRCS, although a very slightly larger number of false alarms and missed oil pixels within the slick are observed, see Figure 4 (a).

Hence, according to the detection map of Figure 4 (b), the extent of the DWH oil spill can be estimated to be approximately 100 km^2 at the SAR acquisition time, i. e., 3 days after the accident.

3.2. Multi–polarization analysis

In this subsection a multi–polarization analysis is undertaken to discuss the sensitivity of HH– and VV–polarized NRCS, σ^0_{HH} and σ^0_{VV}, respectively, to slick–free and oil–covered backscattering. The two intensity channels are jointly used to generate the Pauli false–color RGB images of Figure 5 where the following color–coding is adopted: R (σ^0_{VV}); G (σ^0_{HH}) and B (σ^0_{HH} - σ^0_{VV}). It can be noted that the joint use of VV and HH channels provides further information that can be exploited to gain a better understanding of the scattering processes. The backscattering from metallic targets (mostly due to ships and oil/gas drilling platforms), see brighter spots in Figure 2, is significantly larger than the sea one at both HH and VV polarizations. Sea surface backscattering results in VV–polarized backscattering larger tha the oil–covered area, as expected from the Bragg/tilted–Bragg theory. The

Preprints (www.preprints.org) | NOT PEER-REVIEWED | Posted: 30 May 2018 doi:10.20944/preprints201805.0442.v1

Table 1. Multi–polarization analysis results.

Transect	ROI	σ^0_{VV} (dB)	σ^0_{HH} (dB)	Δ_{VV} (dB)	Δ_{HH} (dB)
Azimuth Direction	Sea	-24.13	-27.34	12.43	10.53
	Oil	-36.59	-37.86		
Range Direction	Sea	-22.62	-25.85	14.40	12.11
	Oil	-37.00	-37.96		

Table 2. Statistical oil–sea separability.

Parameter	HH	VV
Oil–sea JM	0.8232	1.0763
Overlapped area (%)	50	40

smallest difference between VV– and HH–polarized backscattering is achieved within the oil–covered areas. From a physical viewpoint, this can be explained considering that oil layer reduces significantly Bragg scattering waves leading to a noise–like backscattering which results in practically no difference between HH and VV channels.

To provide a quantitative analysis of VV and HH backscattering over slick–free and oil–covered sea surface, σ^0_{VV} and σ^0_{HH} values related to the azimuth– and range–oriented transects, see white dashed lines in Figure 2, are depicted in Figure 6. Values related to the along–range transect are depicted in Figure 6 (a), where one can not that: over slick–free sea surface $\sigma^0_{VV} > \sigma^0_{HH}$ (the difference is about 3 dB) since Bragg scattering applies; within the oiled area, the backscattering is significantly lower than the sea one and there is negligible difference between HH and VV channels (the difference is less than 1 dB). Same comments apply for the azimuth–oriented transect, see Figure 6 (b). The mean values related to slick–free and oil–covered σ^0 values evaluated along with this transect are listed in Table 1 where the contrast Δ, i. e., the slick–free to oil–covered σ^0 ratio, is also listed for both the channels. As expected, the VV–polarized contrast is larger than the HH one (of about 2 dB) due to the larger sea surface backscattering in VV channel.

To further discuss sea–oil backscattering separability, two equal–size Region of Interest (ROIs) kept within the oiled area and the slick–free sea surface are considered and the empirical probability density function (pdf) related to σ^0 values are shown for both the VV and HH channels, see Figure 7. It can be noted that there is a good oil–sea separability at both HH and VV polarization according to the Jeffries–Matusita (JM) distance, see Table 2. The JM distance is defined as $JM = 2(1\text{-}e^{-B})$, where $B = -\ln\left(\sum_{x\in X}\sqrt{(p(x)q(x))}\right)$ is the Bhattacharyya distance between the distribution pixel x belonging to slick–free (p) and oil–covered (q) ROIs [42]. In fact, the minimum JM value, i. e., 0, means that the two distribution are completely overlapped while the maximum JM value, i. e., 2, means totally separated distributions.

Results listed in Table 2 clearly show that the largest oil–sea separation is provided by VV channel (JM = 1.0763) with a 40% overlapping between oil and sea pdfs. However, even when the HH channel performs fine in oil–sea separation (JM = 0.8232) with an overlapping equal to 50%. It can be also observed that the largest separation is provided by the combination of σ^0_{HH} evaluated over oil and σ^0_{VV} evaluated over slick–free sea surface.

Preprints (www.preprints.org) | NOT PEER-REVIEWED | Posted: 30 May 2018 doi:10.20944/preprints201805.0442.v1

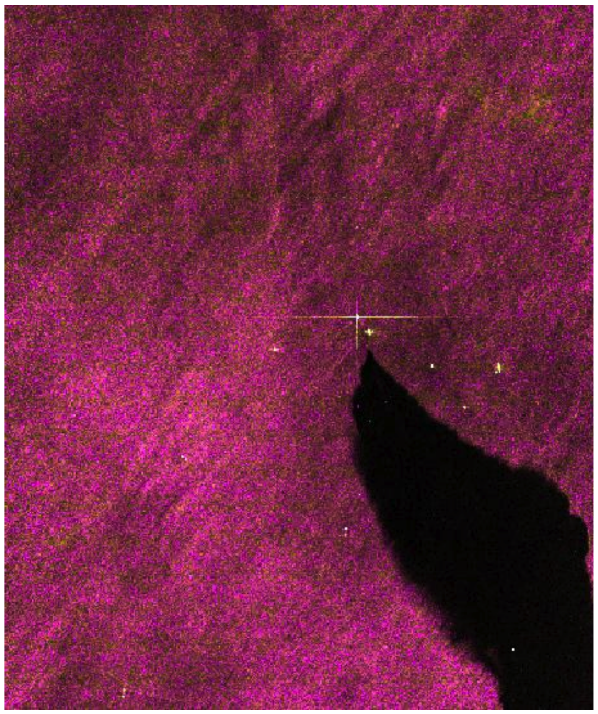

Figure 5. False–color RGB image relevant to the CSK SAR scene collected on 23 April 2010, where the following color–coding is adopted: R $\equiv \sigma^0_{VV}$, G $\equiv \sigma^0_{HH}$ and B $\equiv \sigma^0_{HH} - \sigma^0_{VV}$.

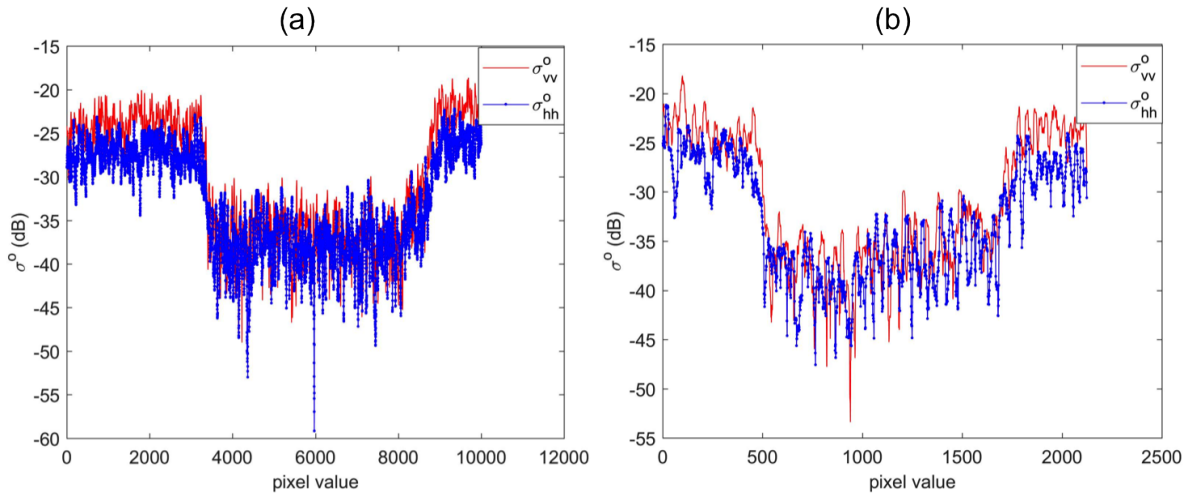

Figure 6. HH– and VV–polarized NRCS values (in dB) evaluated along with the range– (a) and azimuth–oriented (b) transects shown in Figure 2.

Preprints (www.preprints.org) | NOT PEER-REVIEWED | Posted: 30 May 2018 doi:10.20944/preprints201805.0442.v1

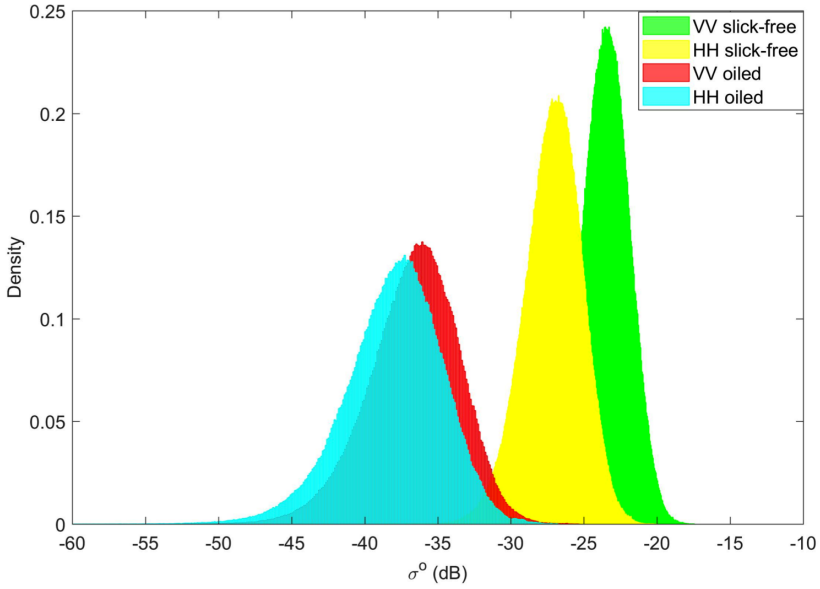

Figure 7. Empirical pdfs related to σ^0 values evaluated over the slick–free and oil–covered sea surface ROIs for both the VV and HH channels.

4. Conclusions

In this study, the capability of multi–polarization CSK SAR data, gathered in dual–polarization PP mode over the Gulf of Mexico, to observe the DWH accidental oil spill is investigated. Experimental results showed that:

- CSK SAR data can be successfully employed to support local authorities in remediation and mitigation activity plans and the sustainability of coastal areas in case of offshore environmental disasters;
- The observation of the DWH oil spill can take full benefits of the fine–resolution, dense revisit time and wide area coverage offered by the CSK satellites constellation;
- The net extent of the DWH oil spill within 3 days of first oil release was about 100 km^2;
- The mean σ^0_{VV} sea–oil contrast is always larger than the σ^0_{HH} one;
- The largest separation is provided by the combination of σ^0_{HH} evaluated over oil and σ^0_{VV} evaluated over slick–free sea surface.

Acknowledgments: This study is partly funded by the Università degli Studi di Napoli Parthenope, project ID DING202. We thank the Italian Space Agency (ASI) that has provided the CSK SAR data under the project ID 1221. Authors would also acknowledge ASI and E–Geos for useful discussions.

Author Contributions: Ferdinando Nunziata and Maurizio Migliaccio conceived and designed the experiments; Andrea Buono and Ferdinando Nunziata performed the experiments and analyzed the data; Ferdinando Nunziata, Andrea Buono and Maurizio Migliaccio wrote the paper.

Conflicts of Interest: The authors declare no conflict of interest. The founding sponsors had no role in the design of the study; in the collection, analyses, or interpretation of data; in the writing of the manuscript, and in the decision to publish the results.

Abbreviations

The following abbreviations are used in this manuscript:

SAR	Synthetic Aperture Radar
DWH	DeepWater Horizon
CSK	COSMO–SkyMed
H	Horizontal
V	Vertical
PP	PingPong
NRCS	Normalized Radar Cross–Section
SCS	Single–look Complex Slant
BP	British Petroleum
NOAA	National Oceanic and Atmospheric Agency
GMF	Geophsyical Model Function
dB	Decibel
GLCM	Gray–Level Co–occurrence Matrix
ASM	Angular Second Moment
RGB	Red Green Blue
ROI	Region Of Interest
pdf	Probability Density Function
JM	Jeffries–Matusita
ASI	Italian Space Agency

References

[1] Costanza, R. The ecological, economic, and social importance of the oceans. *Ecol. Enon.* **1999**, *31*, 199-213.

[2] Visbeck, M. Ocean science research is key for a sustainable future. *Nat. Comm.* **2018**, *9*, 1-4.

[3] Fanning, L.; Mahon, R.; Baldwin, K.; Douglas, S. Transboundary Large Marine Ecosystems. In *Transboundary Waters Assessment Programme (TWAP) Assessment of Governance Arrangements for the Ocean*; Intergovernmental Oceanographic Commission Technical Series 119, United Nations Educational, Scientific and Cultural Organization; Paris, France, 2015.

[4] United Nations. The Sustainable Development Goals Report 2016. United Nations; New York, USA, 2016.

[5] Fingas, M.; Brown, C. E. Review of Oil Spill Remote Sensing. *Spill Sci. Technol. Bull.* **1997**, *4*, 199-208.

[6] Fingas, M.; Brown, C. E. Oil Spill Remote Sensing. In *Handbook of Oil Spill Science and Technology*; Fingas, M., Eds.; Wiley, 2015; pp. 313-356, 978-0-470-45551-7.

[7] Leifer, I.; Lehr, W. J.; Simecek–Beatty, D.; Bradley, E.; Clark, R.; Dennison, P.; Hu, Y.; Matheson, S.; Jones, C. E.; Holt, B.; Reif, M.; Roberts, D. A.; Svejkovsky, J.; Swayze, G.; Wozencraft, J. State of the art satellite and airborne marine oil spill remote sensing: Application to the BP oil spill. *Remote Sens. Environ.* **2012**, *124*, 185-209.

[8] Beyer, J., Trannum, H. C.; Bakke, T.; Hodson, P. V.; Collier, T. K. Environmental effects of the Deepwater Horizon oil spill: A review. *Mar. Poll. Bullet.* **2016**, *110*, 28-51.

[9] Solberg, A. H. S. Remote Sensing of Ocean Oil Spill Pollution. *Proc. IEEE* **2012**, *10*, 2931-2945.

[10] Migliaccio, M.; Nunziata, F.; Buono, A. SAR polarimetry for sea oil slick observation. *Int. J. Remote Sens.* **2015**, *36*, 3243-3273.

[11] Dietrich, J. C.; Trahan, C. J.; Howard, M. T.; Fleming, J. G.; Weaver, R. J.; Tanaka S.; Yu, L.; Luettich Jr., R. A.; Dawson, C. N.; Westerink, J. J.; Wells, G.; Lu, A.; Vega, K.; Kubach, A.; Dresback, K. M.; Kolar, R. L.; Kaiser, C.; Twilley, R. R. Surface trajectories of oil transport along the Northern Coastline of the Gulf of Mexico. *Cont. Shelf. Res.* **2012**, *41*, 17-47.

[12] Cheng, Y.; Liu, B.; Li, X.; Nunziata, F.; Xue, Q.; Ding, X.; Migliaccio, M.; Pichel, W. G. Monitoring of oil spill trajectories with COSMO–SkyMed X–band SAR images and model simulation. *IEEE J. Sel. Topics in Appl. Earth Obs. Remote Sens.* **2014**, *7*, 2895-2901.

[13] Montuori, A.; Nunziata, F.; Migliaccio, M.; Sobieski, P. X–band two–scale sea surface scattering model to predict the contrast due to an oil slick. *IEEE J. Sel. Topics in Appl. Earth Obs. Remote Sens.* **2016**, *13*, 4970-4978.

[14] Brekke, C.; Solberg, A. H. S. Oil spill detection by satellite remote sensing. *Remote Sens. Environ.* **2005**, *95*, 1-13.

[15] Gade, M.; Alpers, W.; Huhnerfuss, H.; Masuko, H.; Kobayashi, T. Imaging of Biogenic and Anthropogenic Ocean Surface Films by the Multifrequency/Multipolarization SIR–C/X–SAR. *J. Geophys. Res.* **1998**, *103*, 18851-18866.

[16] Gade, M.; Alpers, W.; Huhnerfuss, H.; Masuko, H.; Kobayashi, T. Radar signatures of marine mineral oil spills measured by an airborne multi–frequency radar. *Int. J. Remote Sens.* **1998**, *19*, 3607-3623.

[17] Nunziata, F.; Gambardella, A.; Migliaccio, M. On the Mueller Scattering Matrix for SAR Sea Oil Slick Observation. *IEEE Geosci. Remote Sens. Lett.* **2008**, *5*, 691-965.

[18] Migliaccio, M.; Nunziata, F.; Gambardella, A. On the Co–polarised Phase Difference for Oil Spill Observation. *Int. J. Remote Sens.* **2009**, *30*, 1587-1602.

[19] Velotto, D.; Migliaccio, M.; Nunziata, F.; Lehner, S. Dual–polarized TerraSAR–X Data for Oil Spill Observation. *IEEE Trans. Geosci. Remote Sens.* **2011**, *30*, 1587-1602.

[20] Gambardella, A.; Giacinto, G.; Migliaccio, M.; Montali, A. One–class classification for oil spill detection. *Pattern Anal. Applic.* **2010**, *13*, 349-366.

[21] Jones, C. E.; Minchew, B.; Holt, B.; Hensley, S. Studies of the Deepwater Horizon Oil Spill with the UAVSAR Radar. In *Monitoring and Modeling the Deepwater Horizon Oil Spill: A Record-Breaking Enterprise, Geophysical Monograph Series 195*; American Geophysical Union, Washington D.C., 2011; pp. 33-50.

[22] Minchew, B.; Jones, C. E.; Holt, B. Polarimetric Analysis of Backscatter from Deepwater Horizon Oil Spill Using L–band Synthetic Aperture Radar. *IEEE Trans. Geosci. Remote Sens.* **2012**, *50*, 1-19.

[23] Migliaccio, M.; Nunziata, F. On the Exploitation of Polarimetric SAR Data to Map Damping Properties of the Deepwater Horizon Oil Spill. *Int. J. Remote Sens.* **2014**, *35*, 3499-3519.

[24] Garcia–Pineda, O.; Holmes, J.; Rissing, M.; Jones, R.; Wobus, C.; Svejkovsky, J.; Hess, M. Detection of Oil near Shorelines during the Deepwater Horizon Oil Spill Using Synthetic Aperture Radar (SAR). *Remote Sens.* **2017**, *9*, 567-586.

[25] National Oceanographic and Atmospheric Administration Office of Response and Restoration. Deepwater Horizon Oil: Characteristics and Concerns. Available online: http://docs.lib.noaa.gov/noaa_documents/DWH_IR/reports/OilCharacteristics.pdf

[26] National Commission on the BP Deepwater Horizon Oil Spill and Offshore Drilling. Final Report to the President: The Gulf Oil Disaster and the Future of Offshore Drilling. Available online: http://www.oilspillcommission.gov/final-report.

[27] Nunziata, F.; Migliaccio, M. International Oil Spill Response Technical Seminar: Oil Spill Monitoring and Damage Assessment via PolSAR Measurements. *Aquat. Procedia* **2014**, 1-8. Available online: www.sciencedirect.com.

[28] National Oceanic and Atmospheric Administration. Natural Resource Damage Assessment: Status Update for the Deepwater Horizon Oil Spill. Available online: http://www.gulfspillrestoration.noaa.gov.

[29] Yapa, P. D.; Wimalaratne, M. R.; Dissanayake, A. L.; DeGraff Jr., A. How Does Oil and Gas Behave When Released in Deepwater?. *J. Hydro–Environ. Res.* **2012**, *6*, 275-285.

[30] Ivshina, I. B.; Kuyukina, M. S.; Krivoruchko, A. V.; Elkin, A. A.; Makarov, S. O.; Cunningham, C. J.; Peshkur, T. A.; Atlas, R. M.; Philp, J. C. Oil spill problems and sustainable response strategies through new technologies. *Environ. Sci.–Proc. Imp.* **2015**, *17*, 1211-1209.

[31] Vilcaez, J.; Li, L.; Hubbard, S. S. A new model for the biodegradation kinetics of oil droplets: application to the Deepwater Horizon oil spill in the Gulf of Mexico. *Geochem. Trans.* **2013**, *14*, 1-14.

[32] Valentine, D. L.; Fisher, G. B.; Bagby, S. C.; Nelson, R. K.; Reddy, C. M.; Sylva, S. P.; Woo, M. A. Fallout Plume of Submerged Oil from Deepwater Horizon. *P. Natl. Acad. Sci. USA* **2014**, *111*, 15906-15911.

[33] Alpers, W.; Holt, B.; Zeng, K. Oil spill problems and sustainable response strategies through new technologies. *Remote Sens. Environ.*. **2017**, *201*, 133-147.

[34] Zhang, B.; Perrie, W.; Vachon, P. W.; Li, X.; Pichel, W. G.; Guo, J.; He, Y. Ocean Vector Winds Retrieval From C–Band Fully Polarimetric SAR Measurements. *IEEE Trans. Geosci. Remote Sens.* **2012**, *50*, 4252-4261.

[35] Li, X.-M.; Lehner, S. Algorithm for Sea Surface Wind Retrieval From TerraSAR–X and TanDEM–X Data. *IEEE Trans. Geosci. Remote Sens.* **2014**, *52*, 2928-2939.

[36] Ren, Y.; Li, X.-M.; Zhou, G. Sea Surface Wind Retrievals from SIR–C/X–SAR Data: A Revisit. *Remote Sens.* **2015**, *7*, 3548-3564.

[37] Stopa, J. E.; Ardhuin, F.; Chapron, B.; Collard, F. Estimating wave orbital velocity through the azimuth cutoff from space–borne satellites. *J. Geophys. Res.* **2015**, *120*, 7616-7634.

 doi:10.20944/preprints201805.0442.v1

[38] Grieco, G.; Lin, W.; Migliaccio, M.; Nirchio, F.; Portabella, M. Dependency of the Sentinel–1 azimuth wavelength cut–off on significant wave height and wind speed. *Int. J. Remote Sens.* **2016**, *37*, 5086-5104.

[39] Ressel, R.; Frost, A.; Lenher, S. A Neural Network–Based Classification for Sea Ice Types on X–Band SAR Images. *IEEE J. Sel. Topics in Appl. Earth Obs. Remote Sens.* **2015**, *8*, 3672-3680.

[40] Singha, S.; Vespe, M.; Trieschmann, O.; Automatic Synthetic Aperture Radar based oil spill detection and performance estimation via a semi–automatic operational service benchmark. *Mar. Poll. Bullet.* **2013**, *73*, 199-209.

[41] Haralick, R. M.; Shanmugam, K.; Dinstein, I. Textural Features for Image Classification. *IEEE Trans. Syst., Man, Cybern.* **1973**, *6*, 610-621.

[42] Swain, P. H.; Davis, S. M. Remote Sensing. The Quantitative Approach. McGraw–Hill, New York, USA, 1978.